The search for white dwarf binaries

Gian Michle Bravo

Division of Astrophysics
Department of Physics

LUND
UNIVERSITY

2024–EXA233

Degree project of 15 higher education credits
June 2024

Supervisors: Michał Pawlak & Ross Church

Division of Astrophysics
Department of Physics
Box 118
SE-221 00 Lund
Sweden

Abstract

In this thesis, I attempt to categorize variable stars found with the OGLE telescope with the main aim being to find binaries containing white dwarfs. To do this, I combine light curve data from the OGLE telescope [16][11] with data from the large Gaia EDR3 catalogue [3] and a recently published 3-dimensional extinction map [18] to gather the colour and absolute magnitude of the binary stars. Lastly, I use an artificial neural network offered by the `phoebe` binary star software to model the light curves, [5], giving precise orbital parameters that allow for categorization of the binary stars. After this data processing, I find that there are likely no double white dwarf binaries in the OGLE catalogue, while a set of 123 white dwarf and main sequence binaries is identified.

Acknowledgements

I want to thank my supervisors Ross and Michal for being there when I had questions, and listening when I had ideas. I likely gave you magnitudes more work than most students do, and the only excuse that I have for it is that your work was actually helpful.

I want to thank my parents for being interested in what I did and helping me with technical aspects of programming, data analysis and the mathematics I did. Your support was incredible, and I'm very sorry for having left home and not having given you grandchildren yet.

I want to thank my friend Attila, who was always there to listen when I was trying to make sense the data and concepts in front of me. As it turns out, trying to explain something to him was very helpful for actually understanding myself. Furthermore, you helped me with downloading the necessary data using SQL in the first place, and gave me a genuinely good idea for plotting a few months later.

I want to thank the people whom I live with for very often offering food out of politeness that I accepted out of hunger. Especially Savinna. Your cakes are incredible. I hope that you liked the one we baked for you.

Lastly, I want to thank everyone else who I have met for the past five months for being able to stand me as I utterly failed to keep my work to myself.

Popular science introduction

Looking at the night sky, stars appear as single bright points that paint the sky. Yet for many stars, there's more to it. A simple amateur telescope pointed at Alpha Centauri, the second brightest light in the southern skies, reveals that the bright point is in reality composed by two stars in close proximity to each other. In the northern hemisphere, the same can be seen when looking at Albeiro in the constellation Cygnus. Such star systems, with two stars bound together by gravity and spinning around each other are called binary star systems, or simply binaries.

When compared to the size of the universe, the stars Albeiro and Alpha Centauri are very close to Earth. As the distances increase, it becomes more and more difficult, or even impossible, for our telescopes to distinguish between two separate stars. However, binary stars can also be detected through in another way. As with clouds dimming the sun, or the rarer but more accurate Lunar eclipses, an object can pass in front of another and shadow it from sight. In binary stars, the light from one of the stars can be shadowed by the other as it passes in front of it once every orbit. The result is a sudden darkening of the light from a binary, which repeats itself once every orbit.

The second key part to my bachelor project are white dwarfs, the remains of stars that run out of fire. As their name suggest, they are small, faint and white in colour, yet their masses are still quite large, leading to very dense objects. At least, this is what theoretical models tell us. But these same theoretical properties mean that studying white dwarfs has been proven difficult.

As astronomers, we cannot build our own stellar systems and observe how they fare. However, we can look at the sky, observe varied systems and see which of our theoretical models hold... and which are proven wrong. The oscillations in brightness of binary stars reveal lots of information about the binaries, from their relative temperature to their radius, affecting how long the eclipse last. We don't know what happens to binary stars when they die. How many pairs of white dwarf binaries exist, and how they look like, is something which still poses many unknowns.

For the past thirty tears, numerous ground and space telescopes have scanned the night sky and meticulously archived their observations. When put together, they allow unprecedented precision in the identifying of stars. I will be the one taking on this challenge, combining and filtering through decades worth of data in the search for white dwarf binaries.

Contents

Chapter 1

Introduction

1.0.1 Motivation

The aim of this project is to find white dwarf binaries, as well as develop the methodology necessary to accurately categorize binary stars. Over the longer term, both of these results are useful to understand the structure and stellar population about the Galaxy, a field of research called cosmology. They will also give insight in the evolution of binary systems.

Binary star systems are very common in the Galaxy, and the majority of stars are expected to become white dwarfs at the end of their lives. The processes behind the formation of binary white dwarf stars, or other star systems containing white dwarfs, will also benefit from a larger database of objects to study.

Lastly, this project highlights limitations with the current hardware and processes for data gathering, and suggests improvements to make the identification of binary stars even more successful than it currently is.

1.0.2 Binary stars

A considerable part of the bright points visible in the sky are in reality pairs (or, in some cases, triplets) of stars in close proximity to each other. Such pairs of stars are called binary systems, or simply binaries. Binary stars are bound together by gravity. They are also in orbits around each other, thus forming a stable systems.

The period of such orbits depends and on the distance between the two stars in the binary and their masses. Kepler's 3rd law can be used to get a useful relationship between the three, stating

$$P^2 = a^3(m_1 + m_2) \tag{1.1}$$

where P is the period of the orbit in years, a is the semi-major axis in Astronomical Units (1 A.U. is approximately the distance between the Earth and the Sun, defined exactly with a numerical value) and m_1 and m_2 are the masses of the stars in solar masses. Thus, two

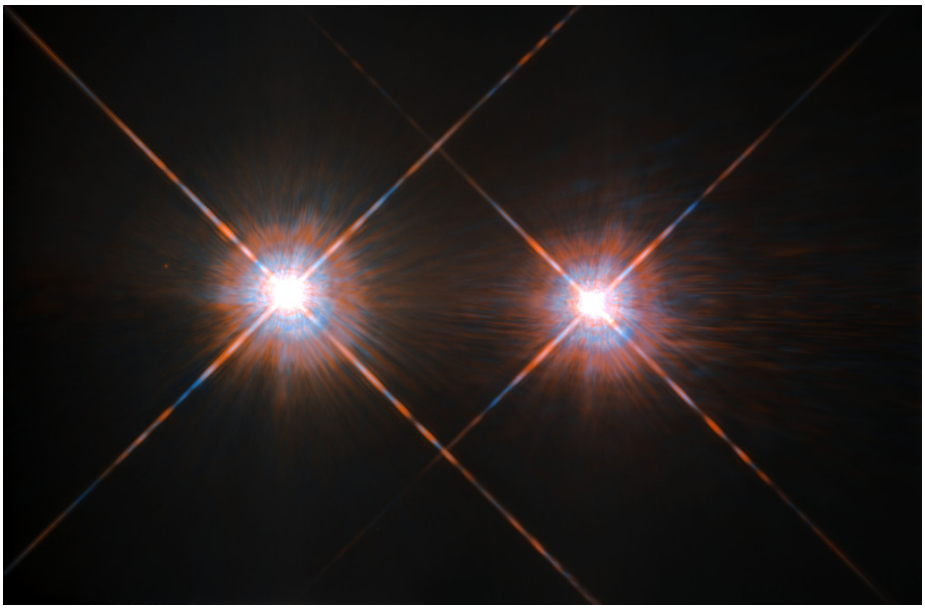

Figure 1.1: An image of Alpha Centauri A and Alpha Centauri B taken by the Hubble Space Telescope, taken from `https://esahubble.org/images/potw1635a/` [10]. For the naked eye, these two stars appear as a single point.

stars weighing 0.5 solar masses Each and 1 A.U. apart would need 1 year to make a full orbit. These units are defined upon the Earth's orbit around the Sun.

There are several different methods to recognize whether a star system is binary or not. The simplest method is to use a telescope powerful enough to resolve the two stars as two separate objects, as seen in figure 1.1 [10]. On a larger scale, more than 1 million binaries have been found with this method [6]. However, the vast majority of stars in binaries are too far from us and too close to each other for our telescopes to resolve them.

A method that has successfully been used for hundreds of thousands of binary stars is the transit method. This relies on the fact that stars move around their orbit. It is thus possible that, once per orbit, one of the binary stars will *eclipse* (partially cover) the second, resulting in a decrease in brightness, as shown in figure 1.2 [8]. By monitoring a large number of stars for a long period of time, many such eclipses can be detected.

Note that for the eclipses to happen, the orbital plane of the binary stars must be sufficiently aligned with Earth. If that's not the case, the stars will simply not pass in front of each other. The largest critical angle α between the orbital plane of the binary and the binary-Earth line is, as seen in figure 1.3,

$$\alpha = \arcsin\left(\frac{R_1 + R_2}{a}\right) = \arcsin\left(F_{sumR}\right) \tag{1.2}$$

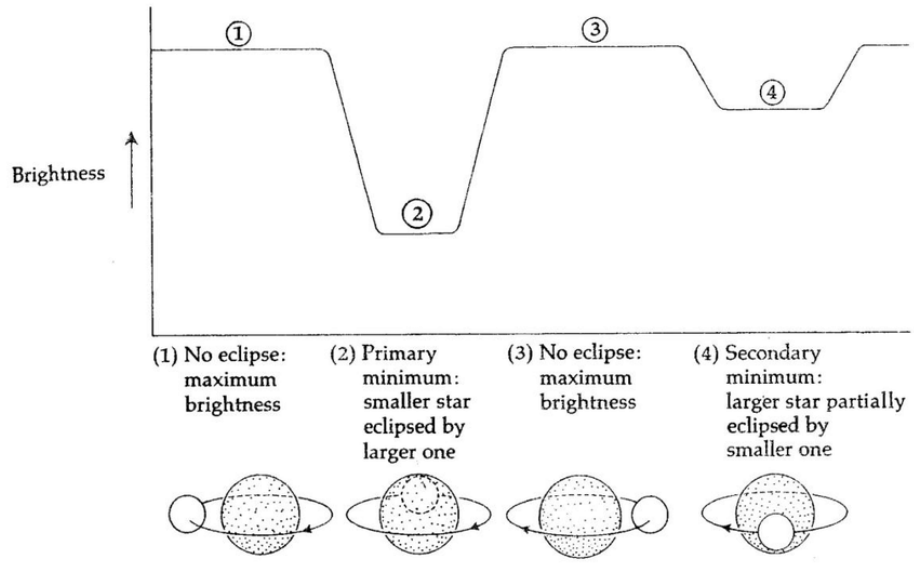

Figure 1.2: A schematic drawing of an eclipsing binary system being observed from Earth. Less light is observed when one of the stars eclipses the other. Taken from [8].

where R_1 and R_2 are the radii of the two stars and a is their distance. Here, it is useful to introduce the sum of the fractional radii $F_{sumR} = \frac{R_1+R_2}{a}$. Assuming that the orientation of the orbital plane is random, the probability of a binary star to show eclipsing events when seen from Earth is then

$$P_E = \frac{2\alpha}{\pi} = \frac{2\arcsin\left(F_{sumR}\right)}{\pi} \tag{1.3}$$

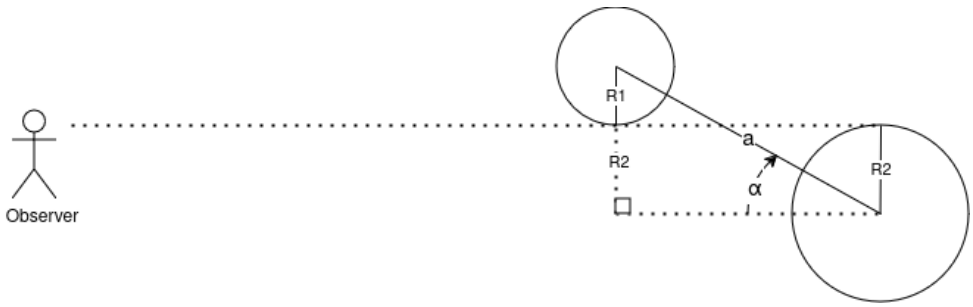

Figure 1.3: A schematic diagram for a binary star system angled at the critical angle, not to scale. For an eclipse to be seen, the angle between the binary-observer line and the plane of the orbit must be smaller than the critical angle α. This angle fulfils $\sin\alpha = \frac{R_1+R_2}{a}$.

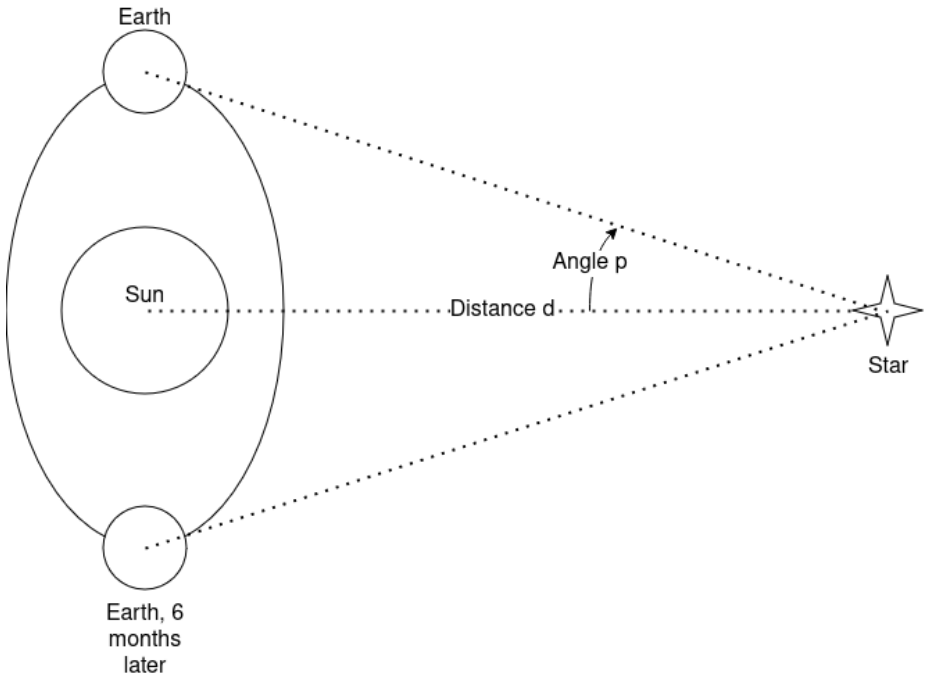

Figure 1.4: A schematic drawing of a parallax angle correlating to the distance of a star. At different times of the year, the star appears to be in a different position in the sky. The closer the star, the more it seems to move, and the larger is ts parallax angle p. Note that for stars other than the sun, p is very small, less than 1 arcsecond.

1.0.3 Parallax distance measurements

Looking at objects from different places gives different results. A simple example can be seen by holding your thumb in front of you and looking at it with your left and right eye, seeing it apparently move against the background.

As a year is twelve months, Eearth will be on opposite sides of the Sun every six months. Images of a stars taken six months apart will therefore show it in slightly different positions. The angle difference seen from opposite sides of the Sun is called the *double parallax angle*. By letting the parallax angle p be measured in arcseconds (1 arcsecond is 1/3600 degrees), the distance d can be calculated from

$$d = \frac{1}{p} \tag{1.4}$$

where d is, by definition, the distance in *parsec*. This is illustrated in figure 1.4. Note that this equation is reliant on the $\sin(x) \simeq x$ approximation, and as such only valid for small angles. Nearly all angles in astronomy are very small.

1.0.4 Magnitude and extinction from space dust

The brightness of an object in the sky can be described in terms of magnitude. This is a negative logarithmic scale, where the fainter an object is, the higher its magnitude. For a star of luminosity L, its apparent magnitude, referred to V in this report, is defined as

$$V = -2.5 \log_{10}(L) + C$$

where C is a constant, previously defined such that the star Vega has a magnitude of 0 as seen from Earth. As later observations have shown that the luminosity of the star Vega varies, this has been set to a numerical value.

Stars, or any object for that matter, appear less luminous when further away. As such, we distinguish between apparent magnitude V, the magnitude that an object appears to have as seen from Earth, and absolute magnitude M, defined as the magnitude of the star seen from a distance of 10 parsecs. Since luminosity decreases with the distance squared, we have that for a star at a distance of d parsecs,

$$V = M - 2.5 \log_{10} \left(\frac{1}{(d/10)^2} \right) = M + 5 \log_{10} \frac{d}{10} \tag{1.5}$$

From theoretical models and observation of nearby objects, we can describe the brightness of some known objects in the night sky. Such objects are known as standard candles, as their absolute luminosity is a "standard" value, regardless of where the objects happen to be [12]. Examples of standard candles are Cepheids and the rarer but brighter type Ia supernovae [12].

Using the absolute magnitudes of these standard candels and their distances (obtained with the parallax angle), it's possible to predict the apparent magnitude of standard candles in the sky. Using telescopes, it is possible to actually measure their apparent magnitude. When this was done on a large scale, the equation 1.5 had a systematic bias. In particular, standard candles further away appeared less bright than predicted. This darkening has been called *extinction.* Furthermore, standard candles close to each other experienced similar levels of extinction.

This effect can be explained by dust in space which absorbs light, similar to the effect of fog on Earth. In general, closer objects experience less extinction, and objects in particularly "foggy" (dusty) regions, such as towards the center of the Galaxy, experience more extinction [18]. The apparent magnitude of a star is then better described by

$$V = M + 5 \log_{10} \frac{d}{10} + A \tag{1.6}$$

where A is the extinction coefficient. Extinction varies depending on the wavelength of the light. In general, dust in space absorbs proportionally more (causes higher extinction for) blue light than red light. By comparing how bright standard candles should appear with

how bright they actually appear at their position, it's possible to create a 3-Dimensional map of how much extinction happens at different points in the sky [18]. Such a map has been used in this bachelor project.

1.0.5 White dwarfs

Looking at the colour-mangitude diagram given by the Gaia telescope (figure 1.5), we see that there are multiple separate regions of stars. The stars in the bottom left group are particularly faint and hot. As such, they are named white dwarfs, often abbreviated as WD. From theorhetical models, these stars as explained as being the remains of stars that finished nuclear fusion [13]. Without the fusion energy pushing the stars apart, gravity caused these stars to collapse into very small, very dense spheres. This collapse also released a lot of energy, leading to the white dwarfs' high temperature [13].

Theoretical models also estimate the masses and radii of white dwarfs. Very generally, white dwarfs have a mass of approximately 1 solar mass M_S and a radius of approximately 0.01 solar radii R_S [13]. A theoretical upper limit to the mass of white dwarfs also exist. At masses over $1.4M_S$,the so called Chandrasekhar limit, it is predicted that white dwarfs collapse into an even smaller and denser neutron stars [14]. So far, no white dwarfs with masses above this limit have been observed [14].

There are numerous reasons why the study of white dwarfs, and double white dwarf binaries in particular, is interesting. Due to their lack of nuclear fusion, WDs slowly cool down, meaning that their temperature gives clear information about the age of a star system. Furthermore, if white dwarfs star happen to gain enough mass, they can cause the extremely bright type Ia supernovae [14], which can happen i.e. when double white dwarf binaries collapse.

The exact mechanisms behind these collapses are however not fully clear yet. As such, finding a larger number of double white dwarf systems is likely to both help the understanding the complex evolution of binary systems and give valuable insight on the stellar population in the Galaxy.

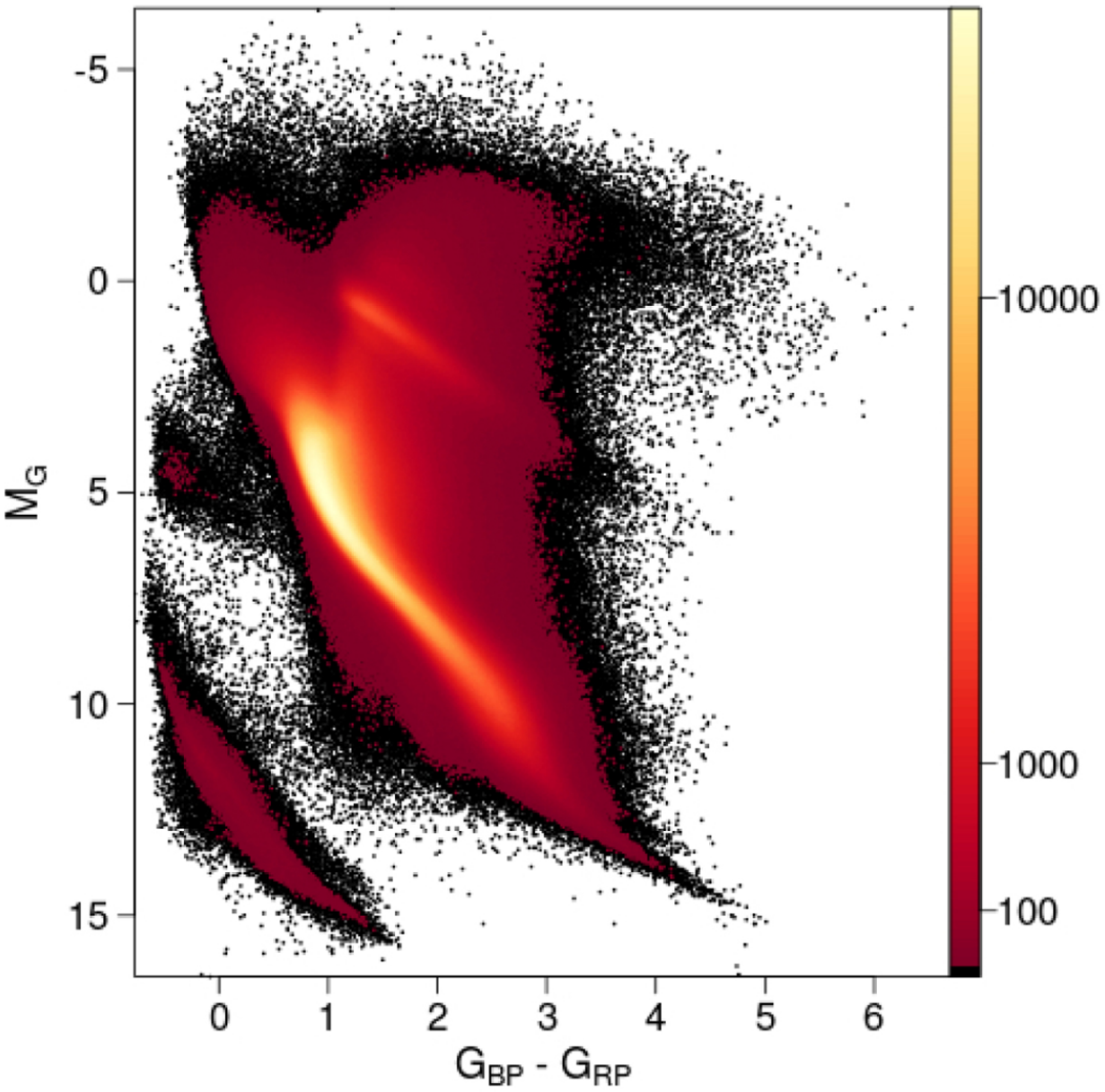

Figure 1.5: The colour-magnitude for stars made from the second data release from the Gaia telescope, with a hotter colour corresponding to a higher concentration of stars. Extinction has been accounted for in this plot. Taken from `https://www.aanda.org/articles/aa/full_html/2018/08/aa32843-18/F1.html` [4].

Chapter 2

Method

2.0.1 Combining datasets

The OGLE public dataset contains data tables and light curves for about 750,000 stars [1]. This data has been taken by the 1.3 meter OGLE telescope in Chile over a period of over 22 years [16][11], and gives repeated measurements for the brightness of stars, making it possible to notice and catalogue how the stars change with time. Particularly, it contains stars in the direction of the Galactic bulge and the Magellanic clouds, where the telescope was pointed. It measures magnitudes in the I (infrared) and V (visible) bands. Normally, there are hundreds to thousands of brightness measurements for each star in the dataset.

This information is often not sufficient to understand what the stars are. Particularly, it's unknown whether the stars are (relatively for stars) faint and (relatively) close, or further away and brighter.

The distance to a star can be calculated from its parallax angle. The Gaia space telescope was launched in 2013 with the aim of mapping as many objects as possible in the entire sky, giving valuable information, key among it being the parallax. [3]. As of now, it has has taken a sufficient number of pictures to give the parallax for more than 1 billion stars, for more than 1 billion stars [3] allowing to, calculate their distance. By combining data from Gaia and from OGLE we get more information about our binary stars [2].

The main hurdle to combining the two datasets is that we do not initially know which star is which. Stars are not artificial objects and do not have easily visible identification codes. However, the two datasets do specify where in the night sky the stars are. As such, we can simply match the coordinates given by the two telescopes. This process is

[1] You can access this catalogue yourself at
`https://ogledb.astrouw.edu.pl/~ogle/OCVS/catalog_query.php`

[2] The Gaia catalogue is also public, though for most applications, it is too large to be dowloaded locally. You can access it at
`https://gea.esac.esa.int/archive/`

referred to as "matching catalogues" and is very common in astronomy research. Note that the universe isn't still, and as such, the apparent position of stars moves with time, especially for nearby stars. This is problematic since the Gaia and OLGE observations happened several years from each other. Luckily, telescopes are capable of observing this movement and predicting with high accuracy the position at any given time. In particular, the calculated positions of the stars during January of the year 2000 (often labeled J2000) was cross-matched.

There is a non-zero error in the position recorded by the telescopes. In this thesis, stars who's positions in the OGLE and Gaia datasets were within 1 arcsecond of each other were put in the new data table. This was done with the CDS crossmatch software [2] [3].

After the crossmatch, objects with an unreliable parallax are discarded as the parallax angle is necessary for making an accurate data analysis. In particular, objects with a negative or nan valued parallax are discarded. Furthermore, objects with a parallax error of more that 100% of the parallax are discarded as well. This is a very relaxed cut chosen for two reasons. First, as white dwarfs are very faint, the parallax error is generally higher for them. Figure 2.1 shows that the number of available stars decreases quickly as this restriction is tightened, particularly in the regions that are relevant to the project. Second, we found that a large group of stars was needed in later data analysis steps to properly show qualitatively different groups of stars. The noise from such a relaxed cut has not been particularly problematic. This leaves 249,965 stars out of the initial 758,762 OGLE variable stars.

2.0.2 Correcting for extinction

To get more precise colour and magnitude values, we use the 3-dimensional reddening map made by Vergely, J.L. and Lallement, Rosine and Cox, N.J.L. in 2022 [18]. It has a resolution of 20 x 20 x 20 parsecs and spans 10 per 10 per 0.8 kiloparsecs. This makes it a box parallel with the galactic plane.

The unit of the map is magnitudes/parsec. As such, to get the total extinction, we integrate over the line of sight from these stars to Earth. The integration is done numerically in 100 discrete steps for each star.

The extinction map gives the extinction in the V (visible) band A_V. We are interested in extinction in the Gaia G-band A_{GP}, as well as for the Blue and Red Gaia bands A_{BP} and A_{RP}. The conversion ratios are given by the paper from N. P. Gentile Fusillo et. al. [7] and are

$$A_{GP} = 0.835 A_V$$

[3] You can access the CDS crossmatch software yourself at
`http://cdsxmatch.u-strasbg.fr/xmatch`

$$A_{BP} = 1.139 A_V$$
$$A_{RP} = 0.650 A_V.$$

Due to the finite size of the box, some objects are outside of it and we cannot find their extinction. After getting the extinction values, 161,499 objects are left from of the 249,965 that passed the previous filtering step. Figure 2.1 show the stars that passed this filtering step in a colour-magnitude diagram, with their colour indicating the relative error in their parallax angle.

2.0.3 Selecting white dwarf candidates

Combining the G-band magnitude with the parallax angle and the extinction allows calculating the absolute magnitude of the objects remaining in the dataset from equation 1.6. A pseudo-colour of these objects can be obtained by comparing the magnitude measured with Gaia's blue and red photometers. This allows plotting the objects in the colour-magnitude diagram seen in figure 2.1.

From this, an apparent problem is seen. Comparing it with a standard colour-magnitude diagram from Gaia, seen in figure 1.5 [4], the stars from the OGLE catalogue do not seem to include some parts of the diagram. Particularly relevant to this thesis, the white dwarf branch in the bottom left of the Colour-Magnitude-Diagram is almost completely missing, or at least not well separated from the main sequence branch.

Regardless, if any WD+WD binaries are present in the dataset, they will be in the bottom left of the figure. Therefore, we make a cut to select those stars, visible as the black line in figure 2.1. The stars that are kept fulfill

$$M_G \geq 7 + 4(G_{bp} - G_{rp}) + (G_{bp} - G_{rp})^2 \tag{2.1}$$

Where M_G is the star's G band absolute magnitude, taking extinction into account, and $(G_{bp} - G_{rp})$ is the star's blue-red colour, taking reddening into account. The exact parameters for this cut were chosen through trial and error, also known as empirically. After the cut, 3,200 variable stars are left out of the 161,499 that passed the previous step. Of them, many aren't binary stars, instead being described by the OGLE catalogue as e.g. Delta Scuti stars or RR lyrae. 1,725 of the remaining stars are binaries.

2.0.4 Analyzing the light curves

The OGLE telescope was meant to capture the variations of star luminosity over time. Thus, for most stars in the catalogue, there are between hundreds to over one thousand magnitude measurements per star, each taken at a different time. These measurements are mostly in the I band with a minority in the V band.

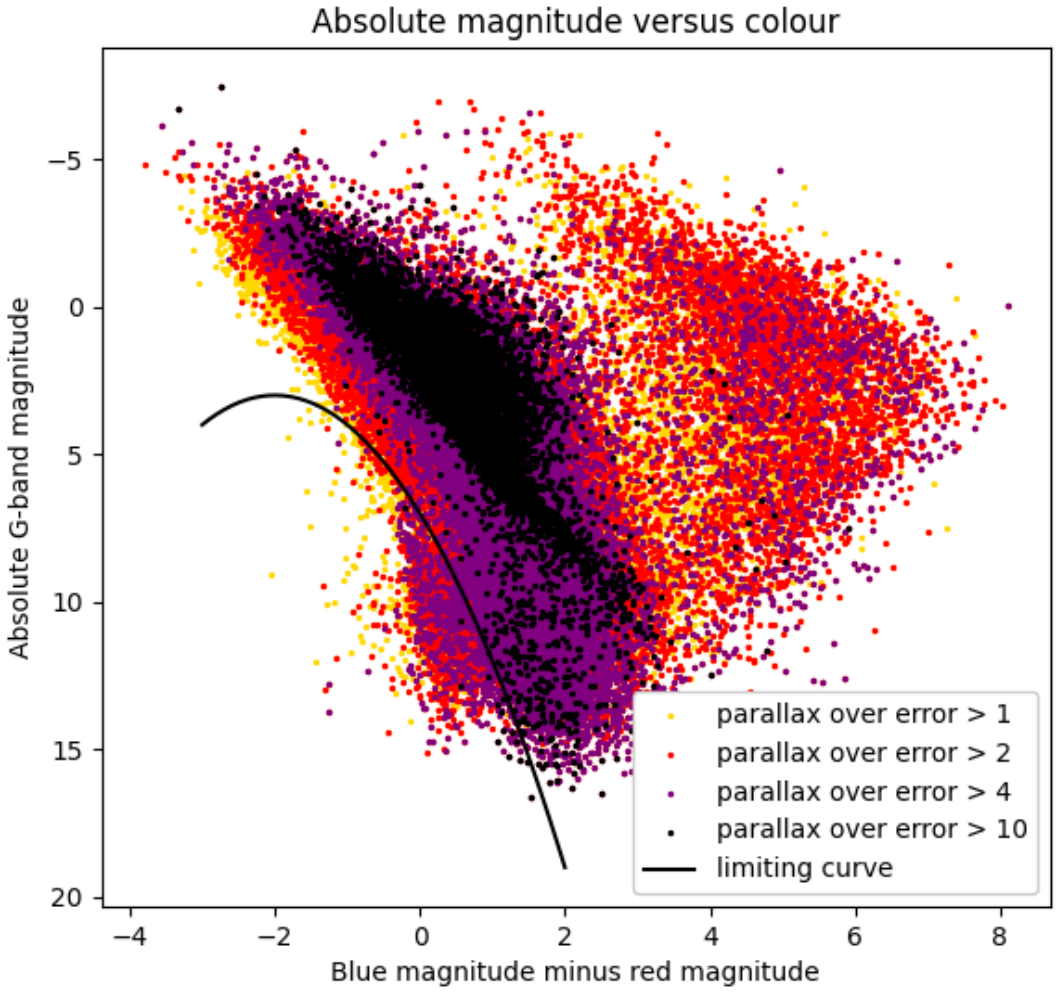

Figure 2.1: Colour magnitude diagram of the variable stars in the OGLE catalogue. Hotter, bluer objects are on the left, with colder objects on the right. More luminous objects are up and fainter objects are down. Extinction has been taken into account. The black line shows the cut made my equation 2.1. The colour of the dots represents their relative parallax errors, with stars with a higher parallax over error (larger certainty) being darker.

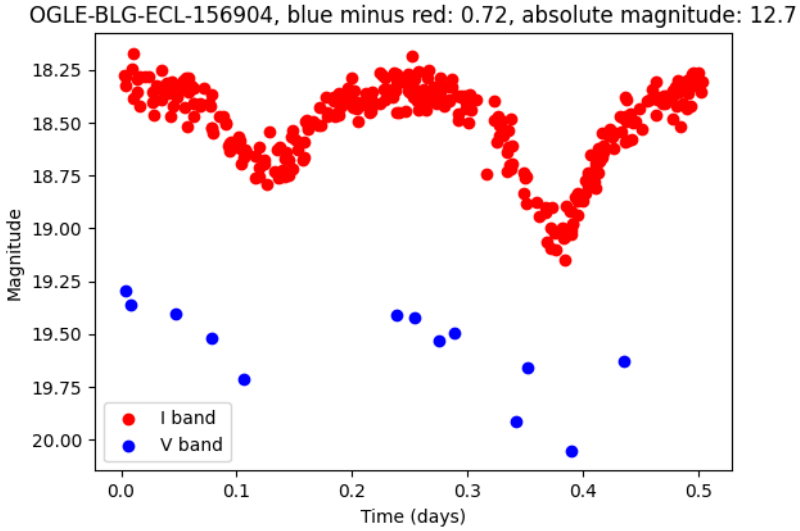

Figure 2.2: An example light curve plot of the binary OGLE-BLG-ECL-156904. It shows that two eclipses happen consecutively. The first, more shallow eclipse, happens when the colder star is eclipsed. The second, deeper eclipse happens when the warmer star is shadowed. These data points were collected over a period of several years [16] and then plotted according to the phase of the binary when they were taken.

Empirically, it can be seen that for many stars observed with OGLE, variations in luminosity are periodic. The OGLE catalogue used in this report is made from such stars. From the period of these stars, it is possible to know the phase (time that has passed since the beginning of a period) at which any given measurement was taken. Plotting the measurements' magnitude versus their phase gives plots such as figure 2.2. Such a plot is commonly referred to as a light curve, despite being often pointy in shape.

The light curves reveal a lot of information about a binary system. Particularly, the width of the eclipses is proportional to the sum of the radii of the objects in the binary, while its depth depends on the temperatures of the two objects. Warmer objects are brighter for a given surface area, and if they are eclipsed by a cooler object, it will result in more light being unable to reach the telescope and a deeper eclipse.

I use the `phoebe 3.63` software [5], to model of the binary stars computationally. Particularly, we use the solver `estimator.ebai`. It is a neural network computer algorithm used to estimate parameters for two-Gaussian function that fits the light curve [5]. A two-Gaussian function is simply a sine curve with two Gaussian functions (also known as normal distributions) subtracted from it. An example of such a model, together with the data used to generate it using `ebai`, is shown in figure 2.3.

Six parameters are given in the two-Gaussian fit. These are:

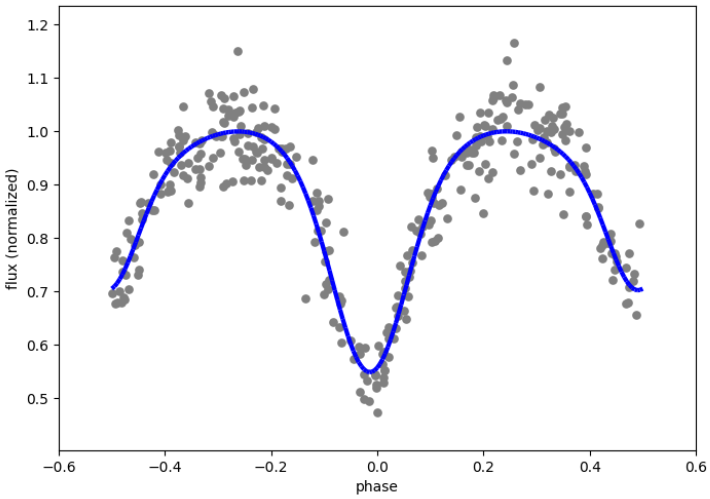

Figure 2.3: A light curve, shown with gray dots, and a fitted two-Gaussian function shown with the blue line. This fit is of the binary OGLE-BLG-ECL-156904, the same binary as 2.2. Compared to figure 2.2, this graph is phase shifted. Another difference is that the y axis displays normalised flux, as opposed to the logarithmic magnitude seen in figure 2.2.

- `t0_supconj`, the zero time point,
- `teffratio`, the ratio of the effective tempeatures of the two stars $\frac{T_1}{T_2}$,
- `requivsumfrac`, the sum of the equivalent fractional radii of the two binary stars. Mathematically, this is $F_{sumR} = \frac{R_1+R_2}{a}$ where a is semi major axis of the binary orbit (for a circular orbit, this is equal to the distance between the two stars),
- `esinw`, the eccentricity multiplied with the sine of the argument of periastron,
- `ecosw`, the eccentricity multiplied with the cosine of the argument of periastron,
- `incl`, the angle between the normal of the orbital plane of the binary and the line between the binary and the Earth.

The parameter `teffratio` is particularly relevant. The effective temperature ratio, henceforth referred to as $R_T = \frac{T_1}{T_2}$ is obtained by comparing the difference in depth of the two eclipses. Two eclipses being significantly different means that the temperatures of the two stars are significantly different.

I expect binaries of two similar stars, such as either two white dwarfs or two main sequence stars, to have $R_T \simeq 1$. For white dwarf and main sequence binaries (WD+MS), we expect the white dwarf to be considerably hotter than the main sequence star, or to be outshone (for equivalent temperature, main sequence stars are several magnitudes brighter

than white dwarfs.)

Chapter 3

Results

For some of the stars, the `ebai` fits fails, returning nan parameters or giving errors. After applying it to the remaining stars, 546 stars are left out of the 1,725 that passed the previous filtering step.

After trying to compare stellar distribution for several parameters, separate groups are seen when plotting the absolute magnitude M_G versus the effective temperature ratio R_T. This plot is shown in figure 3.1. In it, two groups are clearly visible, one with a low and one with a high temperature ratio.

These qualitatively different groups allow us to categorize the binary stars. In particular, we make a cut to select a subgroup of WD+MS binaries. This cut on the M_G and R_T diagram is also shown in figure 3.1. Binaries that are kept fulfil

$$M_G > \begin{cases} 7.5 \text{ for } R_T < 0.6 \\ 7.5 + 800(R_T - 0.6)^3 \text{ for } R_T \geq 0.6 \end{cases} \tag{3.1}$$

This cut removes stars that are too bright as, in testing, some of the bright stars with high temperature differences were found to b main sequence *hot subdwarf* binaries, and not the WD+MS stars that we are interested in. Simplifying, hot subdwarfs are brighter than white dwarfs and fainter than main sequence stars [9], for the same colour. As their name implies, they are also hot [9], meaning that they can have large temperature differences with redder main sequence stars. They can be seen as a small clump the Colour Magnitude Diagram of figure 1.5 for $3 < M_G < 6$, to the left of the image. Due to their brightness, keeping binaries $M_G > 7.5$ should reduce their contamination of the WD+MS group.

From figure 3.1, no obvious white dwarf white dwarf binary (WD+WD) group is seen. Thus, if WD+WD binaries are in that plot, they are mixed with other stars. After manually analysing the most likely candidates (letting $R_T > 0.9$, $B_p - R_p > 0$ and $M_G > 8$), *none* of the stars have the very narrow eclipses that would be expected from WD+WD binaries.

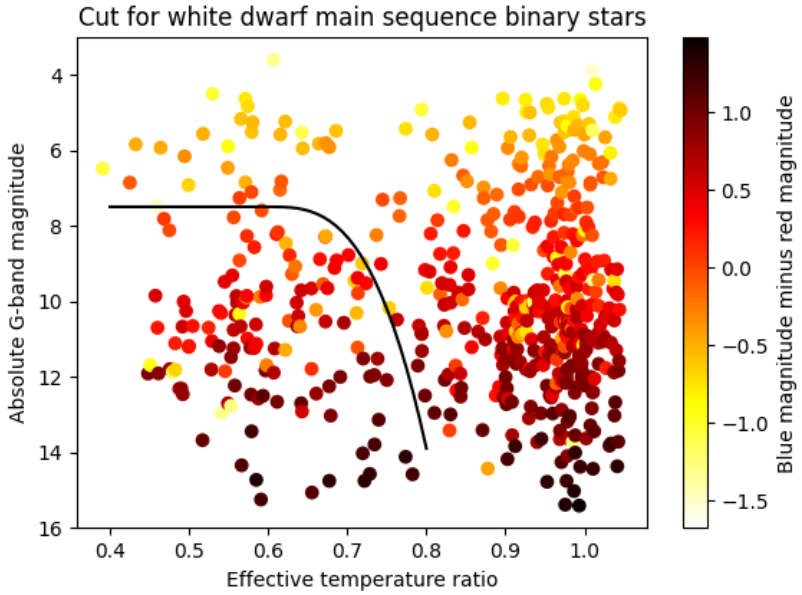

Figure 3.1: A scatter plot of the 546 binaries for which the ebai analysis gave results. The x axis gives the effective temperature ratio R_T between the two stars. Large temperature differences are on the left, smaller temperatures on the right. The Y axis denotes absolute magnitude, with brighter binaries being further up and darker down. A third parameter, the blue-red colour of the binaries, is shown in the colour of the dots, with hotter stars having warmer colours. Two separate groups of binaries can be seen, one of the left and one on the right. Lastly, the black line denotes the temperature ratio/magnitude cut that was made to create the WD+MS dataset.

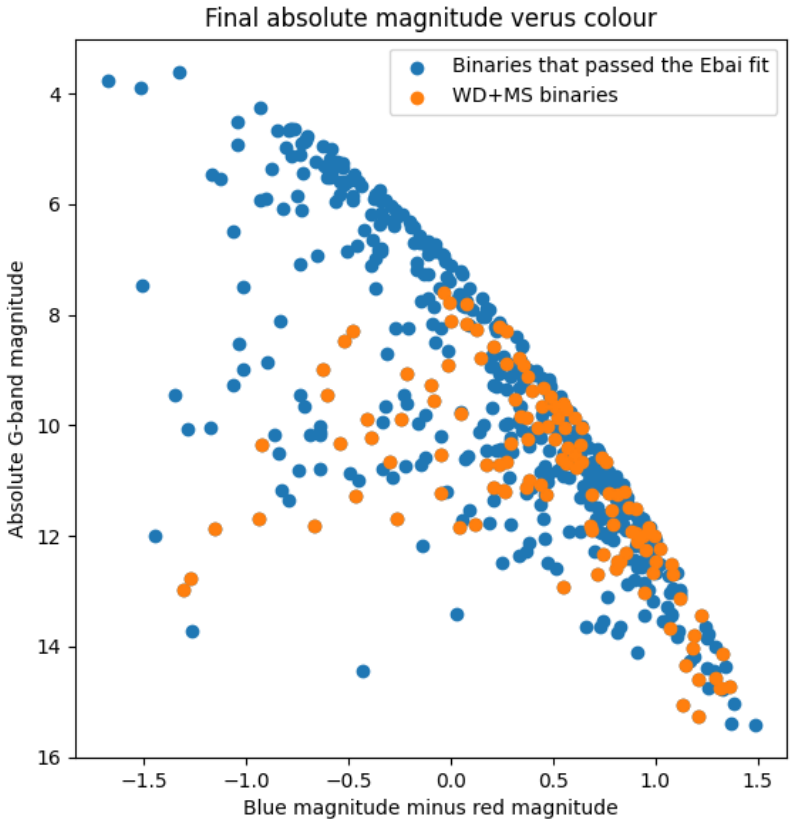

Figure 3.2: The colour magnitude diagram for the 546 binaries that were succesfully categorized with ebai, with extinction accounted. Of them, the binaries now in the WD+MS table are shown with orange dots, while the others are blue.

In total, the WD+MS catalogue contains 123 stars displayed in table A.1. No WD+WD binaries have been identified.

Chapter 4

Discussion

4.0.1 Loss of stars in the Ebai fitting

More than two thirds of the binaries were removed from the dataset during the `ebai` fit. This is not something that would be expected. A possible explenations is that the light curves for which the fit failed were simply too degenerate (too many sets of parameters gave the same result). Furthermore, there was noise in the light curves, which leads to no sets of parameters working perfectly. The last effect is that possible stellar flares would produce data vastly different than what is expected from a binary systems, as seen in the light curve of OGLE-BLG-ECL-000082, figure 4.1. Momentarily, the binary becomes several magnitudes brighter, something that a two-Gaussian model cannot predict. However, there are approximately only 18 stars with large flares in the OGLE catalogue [17].

The solver `ebai` is an artificial neural network, good at solving what it was trained for. It is possible an artificial neural network on a more varied set of light curves will increase its success rate.

4.0.2 WD+MS binaries

The WD+MS found leave many questions. For such a system to exist, a binary system with significantly different star masses is required so that one can finish its nuclear fusion and become a white dwarf while the other is still burning. Between being a main sequence star and a white dwarf, a star will pass the red giant phase [13].

From simple calculations, the stars in our WD+MS systems, are much closer to each other than the radius of a red giant star. In particular, given normal main sequence star radius in the order of 0.1 to 1 R_S and the fractional radius equivalent of the binaries F_{sumR} being between 0.1 and 1 as shown in table A.1, the maximum separation should be in the order of 10 R_S, far smaller than the radius of red giants of $\simeq$100 R_S [13].

This brings up a new question. Did the two stars begin further apart and approach to their

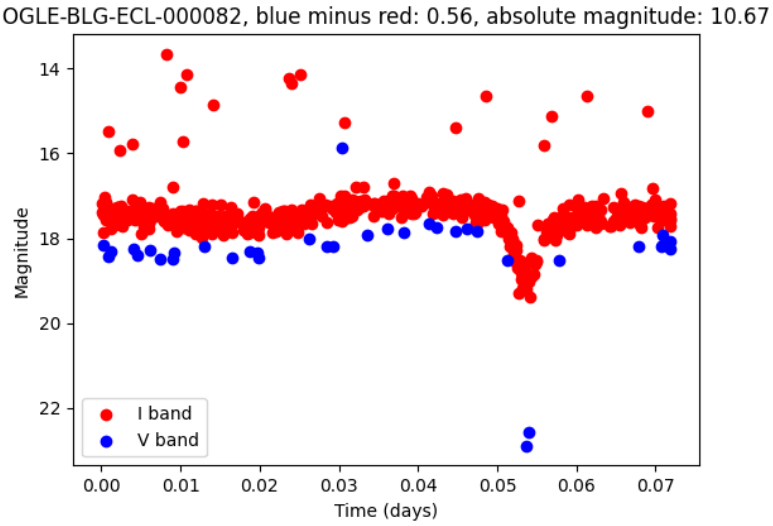

Figure 4.1: A particularly clear example of the light curve of a WD+MS binary, the star OGLE-BLG-000082. The eclipses are very deep, at about 2 magnitudes in the I band and 5 in the V band, showing that one star is a lot hotter and brighter than the other star. Furthermore, this binary shows rare but present observations of highly increased luminosity. These are so called flares, typical of brown dwarf stars, the coldest stars in the main sequence.

current distance after the red giant phase, or was the main sequence star already present *inside* the low density red giant? The 123 WD+MS stars may be used to help show and/or disprove current theories of stellar evolution about such systems.

It is also interesting to know the structure of the WD+MS structure currently. During this project, common-envelope systems were remarkably successful at simulating the light curves of WD+MS binaries. This suggests that a considerable amount of material is not on either of the stars, instead found in the space between them, likely torn off the main sequence star and falling into the extremely dense white dwarfs. An example of such an event may be seen in the star OGLE-BLG-000082 4.1, which has had dramatic increases in brightness while it was being observed by OGLE.

We expect gas falling into the white dwarf to be potentially heated up to very high temperature. As such, these systems may be interesting to observe by X-ray telescopes, especially in those with a large fractional equivalent radius (`requivsumfrac` in the `ebai` parameters.)

4.0.3 Limitations in the OGLE survey for WD+WD binary identification

We can estimate the probability of a binary system to show eclipses from equation 1.3 and use it to make figure 4.2. This explains a large part of the difficulties in finding white dwarf binaries. Unless periods are very short, shorter than can be found in the OGLE catalogue, the probability of a WD+WD star to show eclipses is a lot smaller than for other binary systems with similar magnitudes.

A second reason is seen in figure 4.3. OGLE might be unable to identify eclipses by a WD+WD binary due to these eclipsing lasting a very short time. We will use a theoretical WD+WD binary where each white dwarf has a mass of 1 M_S and a radius of 0.01 R_S. For example, at a period of 0.1 days, an eclipse would last $\simeq$0.8 minutes, or about 50 seconds. The integration time of the OGLE telescope is approximately similar to 100 seconds [16]. Thus, if the OGLE telescope captured such events, it would capture a lot of light from the binary *not* eclipsing during the 100 seconds, leading to a more shallow transit that could easily be mistaken for noise. A period of about 1 day is necessary for the eclipse to be able to last 100 seconds, as seen in figure 4.3.

Furthermore, the chance of capturing either of two 100 second long transits during a full day period is low, or about 1 transit per 400 observations. Considering that most stars in the OGLE catalogue contain "only" hundreds to thousands of points, this would lead to very few eclipsing data points, and once again making it difficult to differentiate such eclipses from noise.

While there is likely no WD+WD binaries in the $\simeq$750,000 stars in the OGLE variable star catalogue, it it is only a subset of the more than 1 billion sources monitored by the OGLE telescope [17]. In particular, the remaining stars have been filtered to show clear periodic variability and not have too large noise [16]. In contrast, the light curve from a WD+WD binary with a period long enough to be observed by OGLE are likely to have very few eclipse observations, distributed almost randomly across the years of OGLE observations, eclipses that could be easily mistaken for noise. Computationally, such light curves may be found in the unfiltered database.

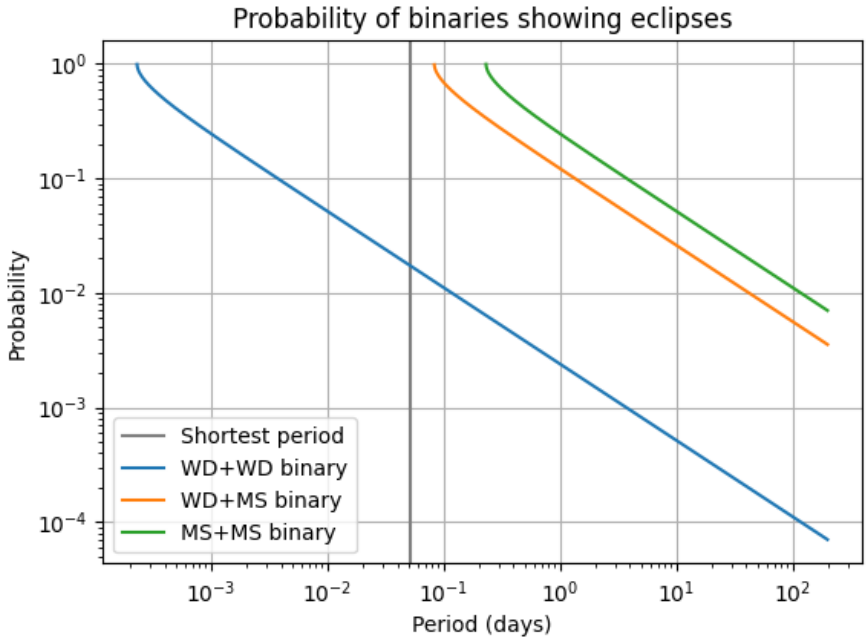

Figure 4.2: An estimation of the probability of an eclipse for different binary periods using equation 1.3. The x axis shows the period of the theoretical binaries, with the y axis showing the probability of eclipsing happening, logarithmic scales. Three different binary stars are modelled: a WD+WD, with star masses of 1 and star radii of 0.01, a WD+MS where the MS star is given a mass of 1 M_S and a radius of 1 R_S (like the Sun), and a MS+MS binary where both stars are Sun-like. The gray line shows the shortest period for a variable star in the OGLE catalogue. We expect systems that contain hot subdwarfs to be in between the WD+WD and the WD+MS line.

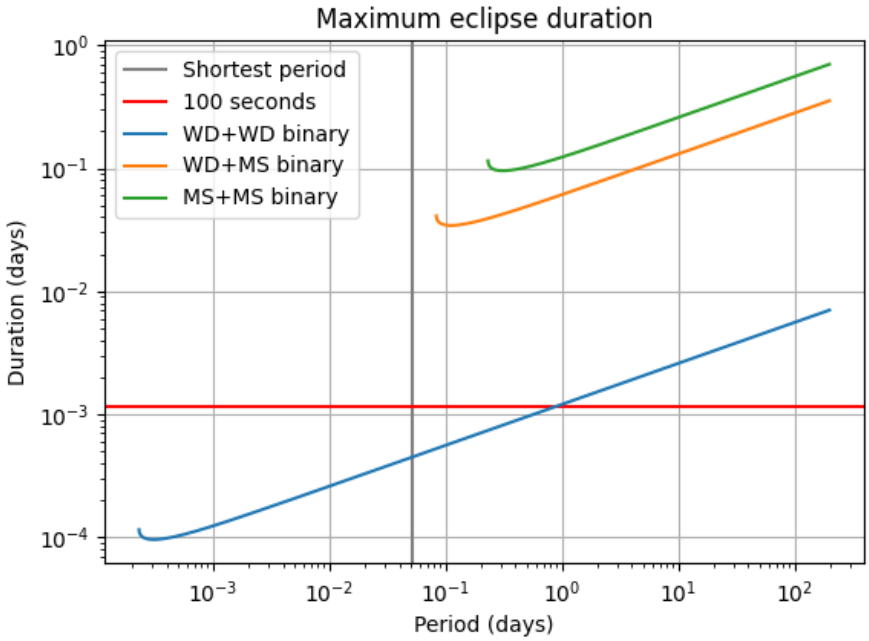

Figure 4.3: The maximum duration of an eclipse for hypothetical binary stars, the same as in figure 4.2. Period of the theoretical binaries is on the x axis, logarithmic scale, equal to that of figure 4.2. They y axis shows eclipse duration, logarithmic scale. The gray line shows the shortest period for a variable star in the OGLE catalogue. The red line shows 100 seconds, or the minimum integration time of the OGLE telescope [16][11].

4.0.4 Considerations for photometric surveys seeking WD+WD binaries

Finding WD+WD binaries with photometric surveys should still be possible in theory. More success may be found using telescopes with *much* shorter integration time. From the simple model seen in figure 4.3, the shortest period of a WD+WD eclipsing star is approximately 20 seconds (at which point the two stars become in contact), with the shortest eclipse duration at approximately 8 seconds.

It is also likely helpful to take observations with a very short cadence. It otherwise may be difficult to know how many orbits happened between observations. Two eclipses observed one day apart might be anywhere between 0.5 and 20,000 orbits apart, with it the true period difficult to estimate, especially if the amount of points is limited and/or if there is uncertainty in when exactly the eclipse happened due to the non-zero integration time.

The short integration time may pose a challenge to telescopes trying to gather enough light. However, some factors would also make a photometric survey easier in other ways. Observation of a star region for a single night, or even for only a part of a night, would reveal most eclipsing WD+WD binaries in the observed sky region. A telescope could have a very narrow field of view and still observe a large part of the sky by not needing to observe the same sky region multiple times.

The Zwicky Transient Facility is a current photometric survey with a considerably shorter integration time than OGLE, at about 30 seconds integration time [1], and has managed to identify approximately 6 WD+WD binaries [15]. These binaries have periods of approximately 1 hour. From the simple model in figure 4.3, corresponds to a maximum period of about 30-40 seconds, which makes sense.

Chapter 5

Conclusion

This thesis shows that with modern parallax surveys, extinction maps and computational tools, it is possible to get parameters about a large number of binaries with high precision. This is possible even with only timed photometric data, with no radial velocity measurements required.

In this thesis, this was used to find a group of 123 WD+MS binaries, and to recognise that no WD+WD are present in the OGLE catalogue used. In general, this approach allows doing categorization of binaries in the OGLE catalogue (and possibly others) on a large scale. From this, it becomes possible to determine population of binary stars in the Galaxy with higher precision than ever, and provide suitable candidates for further research into binary star evolution.

This study also showcased limitations in the current methods, particularly how the exposure time of current telescopes being too long to observe eclipses in ultra-short-period binaries. Suggestions for how to observe them were given. Throughout project, a lot was learned, and the door to further research is now wide open.

Bibliography

[1] Eric C. Bellm, Shrinivas R. Kulkarni, and Graham et. al. The zwicky transient facility: System overview, performance, and first results. *Publications of the Astronomical Society of the Pacific*, 131(995):21, December 2018.

[2] T Boch, FX Pineau, and S Derriere. *CDS xMatch service documentation*, 2021.

[3] A. Brown, A. Vallenari, T. Prusti, J. de Bruijne, C. Babusiaux, M. Biermann, O. Creevey, Dafydd Evans, L. Eyer, A. Hutton, F. Jansen, C. Jordi, Sergei Klioner, U. Lammers, Lennart Lindegren, X. Luri, F. Mignard, C. Panem, Dimitri Pourbaix, and Tomaz Zwitter. Gaia early data release 3. summary of the contents and survey properties. *Astronomy and Astrophysics*, 649, 05 2021.

[4] Gaia Collaboration, C. Babusiaux, Floor van Leeuwen, Martin Barstow, C. Jordi, A. Vallenari, Diego Bossini, Alessandro Bressan, Tristan Cantat-Gaudin, M. Leeuwen, A. Brown, T. Prusti, J. de Bruijne, C. Bailer-Jones, M. Biermann, Dafydd Evans, L. Eyer, F. Jansen, Sergei Klioner, and Tomaz Zwitter. Gaia data release 2: Observational hertzsprung-russell diagrams. 04 2018.

[5] Kyle E. Conroy, Angela Kochoska, Daniel Hey, Herbert Pablo, Kelly M. Hambleton, David Jones, Joseph Giammarco, Michael Abdul-Masih, and Andrej Prša. Physics of eclipsing binaries. v. general framework for solving the inverse problem. *The Astrophysical Journal Supplement Series*, 250(2):34, October 2020.

[6] Kareem El-Badry, Hans-Walter Rix, and Tyler M Heintz. A million binaries from gaia edr3: sample selection and validation of gaia parallax uncertainties. *Monthly Notices of the Royal Astronomical Society*, 506(2):2269–2295, February 2021.

[7] N. P. Gentile Fusillo, P. E. Tremblay, E. Cukanovaite, A. Vorontseva, R. Lallement, M. Hollands, B. T. Gänsicke, K. B. Burdge, J. McCleery, and S. Jordan. A catalogue of white dwarfs in Gaia EDR3. *MNRAS*, 508(3):3877–3896, December 2021.

[8] Mohammad Hani, Mohammad El-Mahameed, Prof edshaker, Hajjawi Co-Supervisor, Prof Mashhoor, and Mashhoor Al-Wardat. *Physical And Orbital Parameter of the Visually Closed Binary System (HIP12552)*. PhD thesis, 01 2014.

[9] U. Heber. Hot Subluminous Stars. , 128(966):082001, August 2016.

[10] Nasa+Esa. Best image of alpha centauri a and b. *ESA Hubble*, 08 2016.

[11] Michal Pawlak, I. Soszyński, A. Udalski, M. Szymański, Lukasz Wyrzykowski, K. Ulaczyk, R. Poleski, P. Pietrukowicz, Szymon Kozlowski, D. Skowron, J. Skowron, P. Mróz, and Aleksandra Hamanowicz. The ogle collection of variable stars. eclipsing binaries in the magellanic system. *Acta Astronomica -Warsaw and Cracow-*, 66, 12 2016.

[12] Dina Prialnik. *An introduction to the theory of stellar structure and evolution*, chapter Helium burning in the core. cambridge university press, 2000.

[13] Dina Prialnik. *An introduction to the theory of stellar structure and evolution*, chapter White dwarfs: the final state of nonmassive stars. cambridge university press, 2000.

[14] Dina Prialnik. *An introduction to the theory of stellar structure and evolution*, chapter The Chandrasekhar mass. cambridge university press, 2000.

[15] Liangliang Ren , Chengyuan Li , Bo Ma , Sihao Cheng , Shun-Jia Huang , Baitian Tang , and Yi-ming Hu . A systematic search for short-period close white dwarf binary candidates based on gaia edr3 catalog and zwicky transient facility data. *The Astrophysical Journal Supplement Series*, 264(2):39, January 2023.

[16] I. Soszyński, Michal Pawlak, P. Pietrukowicz, A. Udalski, M. Szymański, Lukasz Wyrzykowski, K. Ulaczyk, R. Poleski, Szymon Kozlowski, D. Skowron, J. Skowron, P. Mróz, and Aleksandra Hamanowicz. The ogle collection of variable stars. over 450 000 eclipsing and ellipsoidal binary systems toward the galactic bulge. *Acta Astronomica -Warsaw and Cracow-*, 66, 01 2017.

[17] A. Udalski, M. Szymański, and G. Szymański. Ogle-iv: Fourth phase of the optical gravitational lensing experiment. *Acta Astronomica*, 65, 04 2015.

[18] J.L. Vergely, Rosine Lallement, and N.J.L. Cox. Three-dimensional extinction maps: Inverting inter-calibrated extinction catalogues. *Astronomy Astrophysics*, 664, 05 2022.

Appendix A

Total WD+MS table

Table A.1: The 123 stars present in the WD+MS dataset. Present are IDs for OGLE and Gaia catalogues, the extinction and reddening values AG and E(BP-RP) as well as the 6 parameters given by the two-Gaussian fit using ebai.

OGLE	Gaia	AG	E(BP-RP)	t0_supconj	teffratio	requivsumfrac	esinw	ecosw	incl
OGLE-BLG-ECL-000082	4040721003309923840	0.222088	0.130061	-0.015989	0.491711	0.719271	0.060185	0.166556	1.136207
OGLE-BLG-ECL-002332	4107307500400127872	0.333608	0.195370	-0.125823	0.642779	0.608567	-0.371074	-0.056717	1.251524
OGLE-BLG-ECL-004889	4107744143981120384	0.524984	0.307446	-0.137493	0.528163	0.676850	-0.261367	-0.028800	1.290036
OGLE-BLG-ECL-009120	4059122159297658368	0.502693	0.294391	-1.306028	0.711754	0.114424	0.291086	0.314305	1.456484
OGLE-BLG-ECL-011797	4059509698474088832	0.448982	0.262937	-0.141840	0.641684	0.625394	-0.376294	-0.053219	1.263806
OGLE-BLG-ECL-013145	4109863864950380032	0.694042	0.406451	-0.216088	0.556155	0.584350	0.073351	0.064568	1.472819
OGLE-BLG-ECL-014562	4059448989058949376	0.630887	0.369466	-0.075237	0.665448	0.346417	-0.020934	0.014096	1.236625
OGLE-BLG-ECL-015876	4059475343067108608	0.467636	0.273861	-0.234241	0.461243	0.627816	0.035053	0.028018	1.300641
OGLE-BLG-ECL-016949	4059474484001371648	0.410466	0.240380	-0.267224	0.540998	0.532634	-0.274561	-0.083992	1.408366
OGLE-BLG-ECL-025519	4058861884293390976	0.571744	0.334830	-0.745647	0.499980	0.504044	-0.018548	-0.105085	1.502750
OGLE-BLG-ECL-025875	4058862227890859392	0.550029	0.322113	-0.118147	0.482581	0.625903	-0.082086	0.045466	1.232126
OGLE-BLG-ECL-026021	4061253047216108032	0.414388	0.242678	-0.035203	0.739682	0.416743	-0.079049	-0.071051	1.199231
OGLE-BLG-ECL-026963	4117551890797299840	1.195015	0.699835	-0.129035	0.554694	0.648453	0.260901	0.183153	1.294964
OGLE-BLG-ECL-030346	4061189997048414720	0.585085	0.342642	-0.117934	0.597846	0.509820	-0.023599	0.039339	1.094431
OGLE-BLG-ECL-035288	4061395708810684160	0.662744	0.388122	-0.108869	0.556319	0.652657	-0.288497	-0.035596	1.091999
OGLE-BLG-ECL-036957	4061371549619954176	0.538190	0.315179	-0.251769	0.448075	0.615288	0.066436	0.081720	1.344553
OGLE-BLG-ECL-041502	4061754321419176192	0.573029	0.335582	-0.367704	0.450919	0.664056	-0.028566	0.106729	1.147571
OGLE-BLG-ECL-049177	4068250648393402496	0.818957	0.479605	0.121474	0.660498	0.488896	-0.103656	-0.058326	1.228968
OGLE-BLG-ECL-049669	4041229153719789440	0.329032	0.192691	-0.126435	0.524720	0.688816	-0.346976	-0.035086	1.136096
OGLE-BLG-ECL-050595	4060936112947490816	0.631834	0.370020	-0.257694	0.499465	0.533967	-0.047748	-0.030159	1.305680
OGLE-BLG-ECL-051762	4060934772915525760	0.668006	0.391203	-0.744256	0.589876	0.445278	0.045843	0.001723	1.499394
OGLE-BLG-ECL-054042	4061903408288402176	0.623949	0.365403	-0.108872	0.585077	0.672092	-0.002601	0.054111	1.045079
OGLE-BLG-ECL-059904	4118127347737646336	0.717935	0.420443	-0.145714	0.558433	0.670054	0.004962	-0.016199	1.453008
OGLE-BLG-ECL-061746	4068278204928826624	0.751288	0.439976	-0.399373	0.482440	0.482243	-0.017370	0.376227	1.417563
OGLE-BLG-ECL-064193	4053434935362309120	0.343964	0.201435	-0.410487	0.582347	0.544122	0.030200	-0.039771	1.278517
OGLE-BLG-ECL-065022	4117252548789000704	0.789707	0.462475	-0.119623	0.738277	0.671944	0.011798	0.008775	1.441628
OGLE-BLG-ECL-072058	4117361430489579008	0.387341	0.226838	0.091157	0.734460	0.669961	0.006394	0.000891	1.456690
OGLE-BLG-ECL-073040	4068330461837372032	1.193194	0.698769	-0.193790	0.627074	0.634435	-0.014513	-0.037788	1.073749
OGLE-BLG-ECL-074173	4040964927347776640	0.306749	0.179641	-0.120801	0.573728	0.661049	0.009271	-0.019013	1.434661
OGLE-BLG-ECL-081264	4061094717500928512	0.939762	0.550352	-0.138223	0.597291	0.639452	-0.041550	0.171145	1.154550
OGLE-BLG-ECL-089269	4067928560196288512	0.197450	0.115632	-0.456005	0.719553	0.211676	-0.144063	-0.546823	1.418979
OGLE-BLG-ECL-090469	4061025963627951616	0.623636	0.365219	-0.472499	0.545504	0.440741	0.156538	0.096406	1.488441
OGLE-BLG-ECL-097000	4068137020760668032	0.936473	0.548425	-0.590046	0.537906	0.680048	0.010233	-0.021422	1.193432
OGLE-BLG-ECL-110149	4041542166737235840	0.036901	0.021610	-0.072246	0.590893	0.517380	-0.019749	0.044737	1.091034
OGLE-BLG-ECL-115718	4041947512802657536	0.266440	0.156035	-0.168510	0.552910	0.690164	-0.006041	0.019624	1.335052
OGLE-BLG-ECL-119055	4041949776338404096	0.423815	0.248198	-0.144730	0.504717	0.680564	-0.254689	0.088161	1.088594
OGLE-BLG-ECL-119554	4040285360462156672	0.343849	0.201368	-0.119275	0.723891	0.343278	-0.017664	0.055741	1.442858
OGLE-BLG-ECL-122754	4057189286501029120	0.598084	0.350255	-0.791839	0.528937	0.446325	-0.000211	0.278023	1.295566
OGLE-BLG-ECL-127762	4068502780151676416	1.001438	0.586471	-0.155449	0.669408	0.623503	-0.015614	-0.029922	1.342216
OGLE-BLG-ECL-128155	4041657035574875904	0.396726	0.232334	-0.289784	0.559880	0.558026	-0.047121	-0.006158	1.210592
OGLE-BLG-ECL-130396	4068901009543674368	0.712880	0.417483	-0.097353	0.479434	0.640545	-0.047422	0.057586	1.130500
OGLE-BLG-ECL-130503	4068484741280103040	0.736838	0.431514	-0.761321	0.607052	0.469264	-0.193648	0.375522	1.346380
OGLE-BLG-ECL-130924	4040658674786752640	0.352721	0.206563	-0.076346	0.597586	0.589430	-0.077534	0.051436	1.129626
OGLE-BLG-ECL-140021	4041560519032936832	0.179780	0.105285	-0.146425	0.611315	0.654244	-0.141060	-0.031253	1.253178
OGLE-BLG-ECL-141178	4040608101521762176	0.153873	0.090112	-0.407981	0.487580	0.470236	0.005658	-0.093601	1.406872
OGLE-BLG-ECL-143411	4041572063959046272	0.220790	0.129301	-0.113065	0.587634	0.662861	0.009436	0.021132	1.142478
OGLE-BLG-ECL-143472	4043418792546497152	0.516770	0.302635	-0.148493	0.540459	0.660655	0.073660	0.084155	1.374349
OGLE-BLG-ECL-156904	4040615213871423360	0.148182	0.086780	-0.119309	0.549114	0.680041	-0.038986	-0.015909	1.426098
OGLE-BLG-ECL-157193	4043437587303106944	0.515819	0.302078	-0.257007	0.584509	0.560209	-0.041045	-0.066150	1.147134
OGLE-BLG-ECL-167625	4056072796865634304	0.652387	0.382056	-0.107735	0.709113	0.476406	0.261200	0.031833	1.086889

OGLE-BLG-ECL-169287	4040428400013461248	0.323220	0.189287	-0.101462	0.636852	0.182595	0.215092	0.136633	1.203192
OGLE-BLG-ECL-173327	4070578451910908672	0.547057	0.320372	-0.133806	0.490190	0.667546	-0.295004	-0.005205	1.421864
OGLE-BLG-ECL-178512	4040407749804296064	0.045169	0.026452	-0.222889	0.721719	0.603948	0.041079	-0.009658	1.473442
OGLE-BLG-ECL-180541	4043343132438802816	0.459437	0.269059	-0.150878	0.538043	0.649412	0.016585	0.043399	1.298986
OGLE-BLG-ECL-182366	4056107740773442944	0.472803	0.276887	-0.121484	0.654786	0.565667	0.023648	-0.034279	1.245552
OGLE-BLG-ECL-183718	4043223461686961792	0.361370	0.211629	-0.118381	0.557751	0.679740	-0.024745	-0.008883	1.291565
OGLE-BLG-ECL-184275	4056287274724775040	0.662295	0.387859	-0.117963	0.718791	0.580408	0.086239	-0.017525	1.175483
OGLE-BLG-ECL-186809	4043338012760448256	0.057854	0.033881	-0.099875	0.782526	0.461512	0.005977	-0.031021	1.388877
OGLE-BLG-ECL-186876	4044055925188058496	0.638976	0.374203	-0.456513	0.544948	0.479176	0.001533	-0.016623	1.163475
OGLE-BLG-ECL-192029	4063599095728130432	0.642870	0.376483	-0.034321	0.460086	0.502008	-0.382095	-0.550954	1.441393
OGLE-BLG-ECL-192323	4043170612201487616	0.047193	0.027638	-0.052821	0.677230	0.088288	-0.237597	0.402759	1.413966
OGLE-BLG-ECL-197758	4056326754080743040	0.603171	0.353234	-0.102961	0.496184	0.622841	0.019178	0.112541	1.115016
OGLE-BLG-ECL-202217	4042296569201816704	0.415458	0.243304	-0.286496	0.563520	0.533158	0.008182	-0.009880	1.248495
OGLE-BLG-ECL-210078	4037252976067781248	0.310921	0.182084	0.103527	0.695729	0.584045	-0.115098	-0.052006	1.237020
OGLE-BLG-ECL-210769	4043954980476979584	0.612680	0.358803	-0.148701	0.640277	0.599053	-0.078153	0.202686	1.248760
OGLE-BLG-ECL-221245	4042481080900151936	0.451463	0.264390	-0.127348	0.712991	0.572227	0.002554	-0.008047	1.235542
OGLE-BLG-ECL-223366	4069333529874162432	0.801428	0.469339	-0.177680	0.621618	0.574593	-0.081883	0.043345	1.094559
OGLE-BLG-ECL-227940	4037423194240415744	0.568226	0.332769	-0.107358	0.634228	0.644141	-0.003418	-0.024765	1.378334
OGLE-BLG-ECL-233491	4062328708888620800	0.585465	0.342865	-0.140309	0.577457	0.638187	0.023122	-0.002847	1.162690
OGLE-BLG-ECL-235800	4062252121267336448	0.454703	0.266287	-0.135367	0.553071	0.655331	-0.029343	-0.015386	1.337844
OGLE-BLG-ECL-235858	4042012074737700608	0.272541	0.159608	-0.096420	0.691172	0.544396	-0.418176	0.188146	1.395483
OGLE-BLG-ECL-237661	4037336813787900032	0.361302	0.211589	-0.073228	0.638095	0.667800	-0.004528	-0.013421	1.455551
OGLE-BLG-ECL-246704	4042101650562247040	0.052141	0.030535	0.031635	0.773733	0.087882	-0.017545	0.418567	1.485644
OGLE-BLG-ECL-253038	4043914844098276736	0.047414	0.027767	-0.095374	0.584954	0.213607	-0.427527	0.413130	1.428933
OGLE-BLG-ECL-261233	4062512396284535424	0.339452	0.198793	-0.103148	0.749976	0.655852	-0.012653	-0.001484	1.192856
OGLE-BLG-ECL-265887	4050250474862190976	0.610235	0.357371	-0.104393	0.573082	0.641669	0.055335	0.059447	1.176684
OGLE-BLG-ECL-272478	4062391449862852864	0.210654	0.123365	-0.129384	0.593481	0.639296	0.007476	-0.019725	1.147390
OGLE-BLG-ECL-275057	4050157390049261952	0.238300	0.139555	-0.510916	0.492065	0.417273	0.031296	-0.098495	1.468281
OGLE-BLG-ECL-277386	4063328272262446464	0.765223	0.448137	-0.755420	0.572951	0.367971	0.148998	0.124790	1.459289
OGLE-BLG-ECL-280077	4063130944318529152	0.807659	0.472988	-0.518945	0.582489	0.420940	0.092749	0.244112	1.529294
OGLE-BLG-ECL-283873	4062887260825461888	0.708986	0.415202	-2.206522	0.713194	0.235061	-0.277772	0.566558	1.444685
OGLE-BLG-ECL-284321	4038954367324756992	0.441652	0.258644	-0.140800	0.686579	0.587392	0.019751	0.234460	1.316866
OGLE-BLG-ECL-286292	4042648034924795264	0.662487	0.387971	-0.163504	0.641666	0.642808	0.027880	-0.004896	1.406307
OGLE-BLG-ECL-290624	4042569351025263232	0.095209	0.055757	-0.093991	0.679060	0.651804	0.016290	0.037124	1.135683
OGLE-BLG-ECL-302417	4049111823312484864	0.878659	0.514568	-0.123576	0.573138	0.620848	0.011382	-0.006542	1.076540
OGLE-BLG-ECL-303611	4062823046684270720	0.037686	0.022070	-0.290535	0.566387	0.541271	-0.041763	0.054995	1.282872
OGLE-BLG-ECL-315849	4049117806074965504	0.217950	0.127638	-0.503268	0.578404	0.419197	-0.014855	0.027512	1.255897
OGLE-BLG-ECL-325574	4050330941185782528	0.719872	0.421578	-0.326129	0.612228	0.389377	-0.029875	0.394564	1.320586
OGLE-BLG-ECL-333904	4064821198673310592	0.735963	0.431001	-0.186781	0.626076	0.581122	0.023589	0.114364	1.164077
OGLE-BLG-ECL-334290	4049138623869580288	0.339477	0.198807	-0.095141	0.660778	0.651975	0.020636	-0.003986	1.425712
OGLE-BLG-ECL-340152	4042734106007349504	0.615267	0.360318	-0.180338	0.636032	0.544452	0.013575	-0.039191	1.183754
OGLE-BLG-ECL-340497	4039685508139831424	0.931742	0.545655	-0.167393	0.468288	0.612367	-0.030739	-0.022157	1.368220
OGLE-BLG-ECL-343088	4050499578744041472	0.037566	0.022000	-0.007341	0.728499	0.593337	0.020493	0.019478	1.079325
OGLE-BLG-ECL-360189	4039629364277180672	0.654805	0.383472	-0.388374	0.701490	0.463356	0.011843	0.054827	1.368760
OGLE-BLG-ECL-367184	4064767700713620224	0.776712	0.454865	-0.162410	0.493112	0.690176	-0.257910	0.101128	1.140177
OGLE-BLG-ECL-367229	4045720555648330496	1.400279	0.820043	-0.036460	0.672260	0.429678	-0.109293	-0.124330	1.514486
OGLE-BLG-ECL-368139	4048780049788059648	0.621383	0.363900	-0.083857	0.608192	0.652550	-0.002447	-0.025916	1.397900
OGLE-BLG-ECL-368352	4049667149560304512	0.526068	0.308081	-0.098715	0.672470	0.669496	0.009880	0.006942	1.435482
OGLE-BLG-ECL-378621	4052202206727520896	0.308248	0.180519	-0.284040	0.475556	0.595097	-0.041002	-0.014577	1.394926
OGLE-BLG-ECL-382628	4049616846992273152	0.069423	0.040656	-0.115924	0.579017	0.656685	-0.001345	-0.008747	1.066142
OGLE-BLG-ECL-383557	4065413289965692800	0.759782	0.444950	-0.092347	0.713547	0.471055	-0.007730	-0.059143	1.209435
OGLE-BLG-ECL-387078	4065584465982471808	0.762427	0.446499	-0.456173	0.654605	0.529720	0.067515	-0.014171	1.350073
OGLE-BLG-ECL-387779	4045482923721103104	0.698399	0.409002	-0.104296	0.560601	0.666626	-0.024743	-0.008776	1.367721
OGLE-BLG-ECL-389012	4049802355168839040	0.703304	0.411875	-0.065416	0.610492	0.366972	0.079717	0.142040	1.255586
OGLE-BLG-ECL-390640	4052647341489162624	0.440309	0.257858	-0.131623	0.728879	0.613552	-0.036067	0.056168	1.141336
OGLE-BLG-ECL-392889	4049426184799207296	0.325873	0.190841	-0.090482	0.734154	0.409121	-0.016820	-0.043486	1.233058
OGLE-BLG-ECL-395023	4045492097776883840	0.367063	0.214963	-0.077263	0.596636	0.608610	0.017194	-0.016517	1.360536
OGLE-BLG-ECL-396315	4065296844749871488	0.956837	0.560351	-0.073572	0.622318	0.518654	-0.133538	-0.106564	1.364987
OGLE-BLG-ECL-398684	4049314515507086208	0.698648	0.409148	-0.449327	0.457469	0.606671	-0.159738	-0.199006	1.187194
OGLE-BLG-ECL-399454	4052650468228764416	0.094935	0.055597	-0.091787	0.516990	0.691002	-0.110949	-0.013966	1.360661
OGLE-BLG-ECL-403583	4052328581873788544	0.636773	0.372912	-0.169313	0.568281	0.140956	0.154384	0.154777	1.258763
OGLE-BLG-ECL-404414	4049763734750141312	0.531252	0.311116	-0.110013	0.565089	0.640705	0.016325	-0.028577	1.288189
OGLE-BLG-ECL-408978	4049579910245018112	0.399385	0.233892	-0.050711	0.677123	0.537028	0.155188	-0.092006	1.406405
OGLE-BLG-ECL-409124	4065229843286956544	0.858367	0.502684	-0.189047	0.563728	0.683022	-0.012468	-0.013425	1.429249
OGLE-BLG-ECL-410780	4053067148770455168	0.757958	0.443882	-0.081790	0.683836	0.408926	-0.084575	-0.058382	1.306439
OGLE-BLG-ECL-414806	4053202109546706560	0.681218	0.398941	-0.095417	0.674961	0.443406	-0.029509	0.181247	1.366760
OGLE-BLG-ECL-416418	4051485569993765888	0.047772	0.027977	-0.082574	0.655359	0.456874	0.029771	0.061862	1.210559
OGLE-BLG-ECL-416440	4052749218107476608	0.872559	0.510996	-0.194314	0.591800	0.586159	0.004732	-0.012503	1.127117
OGLE-BLG-ECL-419747	4052756498057870848	0.968213	0.567014	-0.105978	0.475095	0.668916	-0.285312	-0.012382	1.463134
OGLE-BLG-ECL-420040	4051074627527086464	0.507825	0.297397	-0.084135	0.720144	0.658867	-0.011961	-0.001053	1.079967
OGLE-BLG-ECL-424295	6761363608770609152	1.273600	0.745856	-0.685963	0.556394	0.418331	0.090383	0.037306	1.414328
OGLE-BLG-ECL-424987	6760097486743454848	0.978035	0.572765	-0.471808	0.630003	0.388991	0.071676	0.003221	1.470456
OGLE-BLG-ECL-425051	6760813028296198528	1.244599	0.728873	-0.255040	0.672719	0.485800	0.020409	-0.034615	1.455071